GEODYNAMICS & TECTONOPHYSICS
Published by the Institute of the Earth's Crust, Siberian Branch, Russian Academy of Sciences

RECENT GEODYNAMICS

2022 VOLUME 13 ISSUE 1 ARTICLE 0570

ISSN 2078-502X

DOI: 10.5800/GT-2022-13-1-0570

LONG-TERM CHANGES IN CRUSTAL MOVEMENTS AND DEFORMATIONS BEFORE AND DURING THE 2016 KUMAMOTO EARTHQUAKE SEQUENCE

V.I. Kaftan ✉, V.N. Tatarinov, R.V. Shevchuk

Geophysical Center of the Russian Academy of Sciences, 3 Molodezhnaya St, Moscow 119296, Russia

ABSTRACT. The Kyushu Island, as well as whole Japanese archipelago, is equipped with dense GPS network (GEONET). It allows us to track the movements and deformations of the earth's surface over long-term time intervals. In this study, based on daily determinations of the coordinates of GPS stations, analysis has been made on long-term trends in the accumulation of movements and deformations in large areas of the Kyushu Island before the series of April 14–16, 2016 Kumamoto earthquakes to identify deformation precursors and locked, immobile fault zones. The study of the seismic deformation process was performed using the data from 70 continuous permanent GPS stations for the period 2009–2016.

The movement and deformation features found characterize the kinematics of the axial zone of the south-western part of the island arc of the Japanese archipelago. The combination of coseismic compression and uplift in the center of the formed triad of deformation extrema and the consistency between subsidence and extensions at its edges demonstrate the mechanism of growth of the central region of the island arc under compression and the role of volcanism. Of particular interest in the context of the development of movements and deformations during the generation of the Kumamoto earthquakes is the behavior of the minimum displacement moduli of the GNSS sites. Analysis of their kinematics shows the formation of a zone of minimum displacements, in which subsequent strong seismic events were localized. It is shown that rather dense and extensive GNSS networks allow observing and studying the seismic-deformation process at the stages of seismic generation, discharge and relaxation, thereby providing an empirical basis for the development of models for predicting large seismic events.

KEYWORDS: earth's surface deformation; GPS; fault locking; slip deficit; earthquake prediction

FUNDING: This work was conducted in the framework of budgetary funding for the Geophysical Center of RAS, approved by the Ministry of Science and Higher Education of the Russian Federation.

RESEARCH ARTICLE

Received: September 4, 2021
Revised: November 16, 2021
Accepted: December 13, 2021

Correspondence: Vladimir I. Kaftan, kaftan@geod.ru

FOR CITATION: Kaftan V.I., Tatarinov V.N., Shevchuk R.V., 2022. Long-term changes in crustal movements and deformations before and during the 2016 Kumamoto earthquake sequence. Geodynamics & Tectonophysics 13 (1), 0570. doi:10.5800/GT-2022-13-1-0570

ДОЛГОВРЕМЕННЫЕ ИЗМЕНЕНИЯ ДВИЖЕНИЙ И ДЕФОРМАЦИЙ ЗЕМНОЙ КОРЫ ДО И ВО ВРЕМЯ СЕРИИ ЗЕМЛЕТРЯСЕНИЙ КУМАМОТО (2016 г., ЯПОНИЯ)

В.И. Кафтан, В.Н. Татаринов, Р.В. Шевчук

Геофизический центр РАН, 119296, Москва, ул. Молодежная, 3, Россия

АННОТАЦИЯ. На острове Кюсю, как и на всем Японском архипелаге, функционирует густая перманентная сеть GPS (GEONET), которая позволяет отслеживать движения и деформации земной поверхности на многолетних временных интервалах. В настоящем исследовании по суточным определениям координат станций GPS анализируются долгопериодические тенденции накопления движений и деформаций на значительной территории о-ва Кюсю перед серией землетрясений Кумамото (14–16 апреля 2016 г.) с целью выявления деформационных предвестников и поиска неподвижных «запертых» зон разломов. Для изучения сейсмодеформационного процесса использованы данные непрерывных GPS-наблюдений 70 непрерывнодействующих станций за период 2009–2016 гг.

Выявленные особенности движений и деформаций характеризуют кинематику осевой зоны юго-западной части островной дуги Японского архипелага. Сочетание косейсмических сжатия и подъема в центре образованной триады экстремумов деформации и согласованность опусканий с растяжениями на ее краях демонстрируют механизм роста центральной области островной дуги в условиях сжатия и роль вулканизма. Наибольший интерес в отношении развития движений и деформаций в процессе подготовки землетрясений Кумамото представляет поведение минимальных модулей смещений пунктов глобальных навигационных спутниковых систем (ГНСС). Анализ их кинематики показывает образование области минимальных смещений, в которой были локализованы последующие сильные сейсмические события. Показано, что достаточно плотные и обширные сети ГНСС станций позволяют наблюдать и изучать сейсмодеформационный процесс на стадиях сейсмической подготовки, разрядки и релаксации, представляя тем самым эмпирическую основу для разработки моделей прогнозирования крупных и сильных сейсмических событий.

КЛЮЧЕВЫЕ СЛОВА: деформация земной поверхности; GPS; запирание разлома; дефицит смещения; прогноз землетрясений

ФИНАНСИРОВАНИЕ: Работа выполнена в рамках государственного задания Геофизического центра РАН, утвержденного Минобрнауки РФ.

1. INTRODUCTION

At present, the movements of the earth's surface are firmly monitored by means of global navigation satellite systems (GNSS) with sub-centimeter accuracy. The global GNSS observational network contains about 20 000 permanent stations. The most densely spaced stations are typical for the territories of the Japanese archipelago, North America, and Europe. Some stations have been in operation for over three decades. Thanks to the open information service provided by the Geodetic Laboratory of Nevada (USA), time series of precise spatial coordinates of permanent GNSS stations with a daily temporal resolution are now available to researchers [Blewitt et al., 2018]. These stations allow tracking changes in the earth's surface motion at all stages of the seismic cycle, in the time interval covered by continuous observations. In many cases, it is possible to study the process of accumulating deformations over the years or even the first decades before strong events at the final stage of the interseismic phase. This allows us to detect and study deformation precursors of earthquakes [Kaftan, Melnikov, 2018], as well as the spatial migration of deformations that disturb and accompany seismic events [Kaftan, Melnikov, 2019]. It could be argued that rather dense and extensive networks of permanent GNSS stations allow observing and studying the seismic-deformation process at the stages of seismic generation, discharge, and relaxation, thereby providing an empirical basis for the development of models to predict strong seismic events.

In the region of the Japanese archipelago, the strongest earthquakes with M>8 occur mainly in the area of oceanic trenches. These territories are not yet accessible for high-precision repeated geodetic measurements, but the corresponding technologies are already being developed and, due to their decimeter accuracy, mainly applied to the study of, coseismic shifts of the seabed and early warning of tsunamis [Yamagiwa et al., 2015; Yang, Qin, 2021]. At the same time, however, Japan destructive earthquakes with M<8 also occur on island territories. Examples of such seismic events include a series of 2016 Kumamoto earthquakes. The first foreshock of M_w6.5 was recorded on April 14, 2016 at 21:26 UTC. The epicenter was located at a depth of 12 km northwest of the city of

Kumamoto, directly at the junction of the Hinagu and Futagawa fault systems [Kato et al., 2016]. In the following hours, at least another 11 shocks were recorded at a magnitude of more than M_w4.5, with the largest of which (M_w6.4) struck farther south, along the strike of the Hinagu fault system. The main shock M_w7.3 was recorded on April 16 at 1:25 UTC at a depth of ~10 km.

On the territory of the Kyushu Island, which experienced a series of these events, there is a dense network of continuous GNSS observations GEONET [Sagiya, 2004; Kawamoto et al., 2016], which is a part of the International GNSS Service (IGS) [Johnston et al., 2017]. Before these earthquakes, the stations accumulated nearly seven years of coordinate time series obtained from daily continuous measurements according to the technology described below. Therefore, the place of the 2016 Kumamoto earthquake series is considered unique experimental area.

The deformations behavior and movements of the earth's surface based on the GPS and remote sensing data are rather thoroughly studied. Co- and post-seismic deformations based on GPS observations were considered in a number of works [Kawamoto et al., 2016; Tanaka et al., 2019; Kubodera et al., 2017; Moore et al., 2017; He et al., 2019; Dahmen et al., 2020]. However, so far there is a lack of publications related to the analysis of the spatiotemporal evolution of preseismic movements and deformations of the earth's surface over a seven-year time interval with a daily recording frequency over a large area. In this regard, we have initiated our own study.

2. OBSERVATION DATA

Experience in analyzing the movements and deformations of the earth's surface in areas of occurrence of strong earthquakes, as well as in zones of active volcanism [Kaftan, Rodkin, 2019; Kaftan, Melnikov,

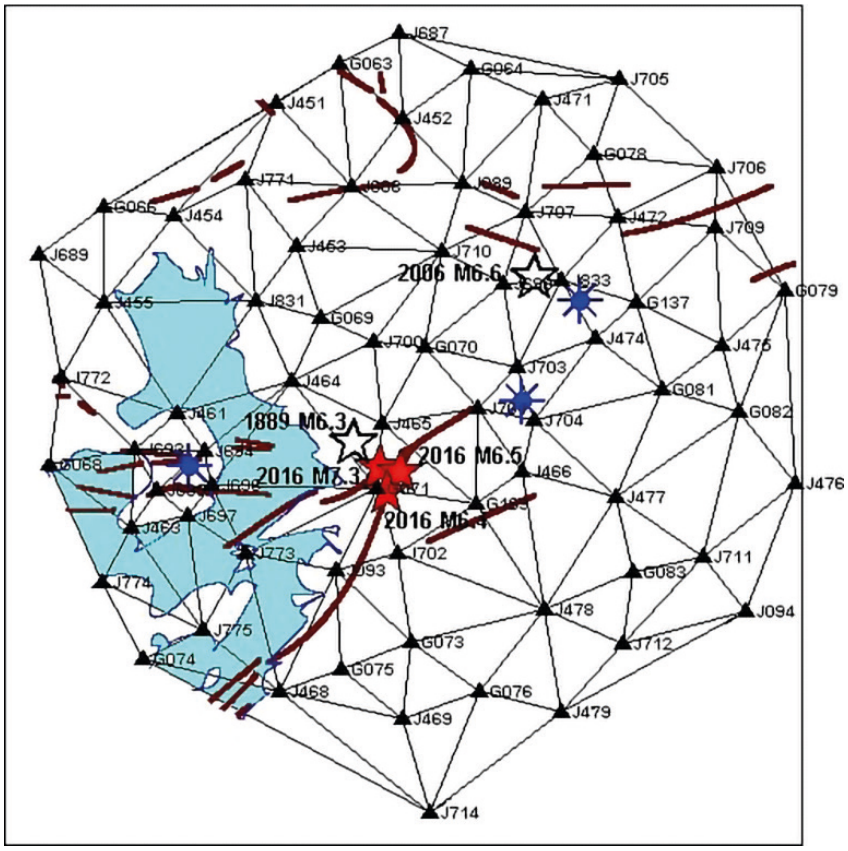

Fig. 1. Configuration of finite elements of a network of permanently operating GPS stations (black triangles with site names). The tectonic setting is generally presented from [Active Fault Database of Japan, 2021].
The brown lines are tectonic faults. Epicenters of seismic events: white stars are historical earthquakes in the area, red stars are strong earthquakes of the 2016 Kumamoto series, blue eight-pointed stars are active volcanoes. The blue area is the sea surface.

Рис. 1. Конфигурация конечных элементов сети непрерывнодействующих GPS-станций (черные треугольники с названиями пунктов). Тектоническая обстановка по данным [Active Fault Database of Japan, 2021] обобщенно.
Коричневые линии – тектонические разломы. Эпицентры сейсмических событий: белые звездочки – исторические землетрясения в районе, красные – сильные землетрясения серии Кумамото 2016 г., синие восьмиконечные звездочки – активные вулканы. Голубая поверхность – морская акватория.

2019] shows that the dimension of control networks should be neither too small nor constrained only by the size of the epicentral zones of foreshocks and aftershocks of major events. Local geodetic observations in the immediate vicinity of the epicentral zones and external manifestations of volcanism do not provide the full picture of the corresponding deformation process, missing some important aspects. Predictive monitoring networks should cover territories with a radius exceeding the length of the fault that ruptures in a certain-magnitude earthquake [Riznichenko 1992].

To study the seismic-deformation process, we used the data of continuous GPS observations from 70 permanently operating stations, with a daily recording interval. The time series of station coordinates were obtained using a precise positioning strategy – Precise Point Positioning (PPP), with precise ephemeris and GPS satellite clock correction, as well as other accurate products of the International GNSS Service. The time series used contain the average daily coordinates in the IGS14 reference system [Blewitt et al., 2018]. The accuracy of determining the spatial position of a point for this strategy is estimated as subcentimeter. The observation gaps were filled with coordinate values interpolated using Hermite splines. The configuration of the control geodetic network is shown in Fig. 1.

The area covered by the network observations has a diameter of about 180 km and includes the epicenters of both recent and the above-mentioned historical events. It should be noted here that in 1889, in the immediate vicinity of the epicentral zone of the 2016 earthquakes series, there occurred a rather strong (M6.3) earthquake (Fig. 1). This fact allows us to make assumptions about the duration of a cycle of sequential seismic events studied here and the time of accumulation of elastic deformations in the earth's crust.

The initial epoch T_0 of determining the movements and deformations from the GNSS data was recorded on January 1, 2009, at more than a six-year observation interval before the earthquakes.

3. TECTONIC SETTING AND SEISMICITY

The main tectonic object that provides tectonic mobility of the study area is the subduction zone of the Philippine tectonic plate [Nakajima, Hasegawa 2007].

The tectonics of the area is determined by two fault zones, Hinagu and Futagawa (Fig. 2), to which 35–40° junction the seismic events under consideration

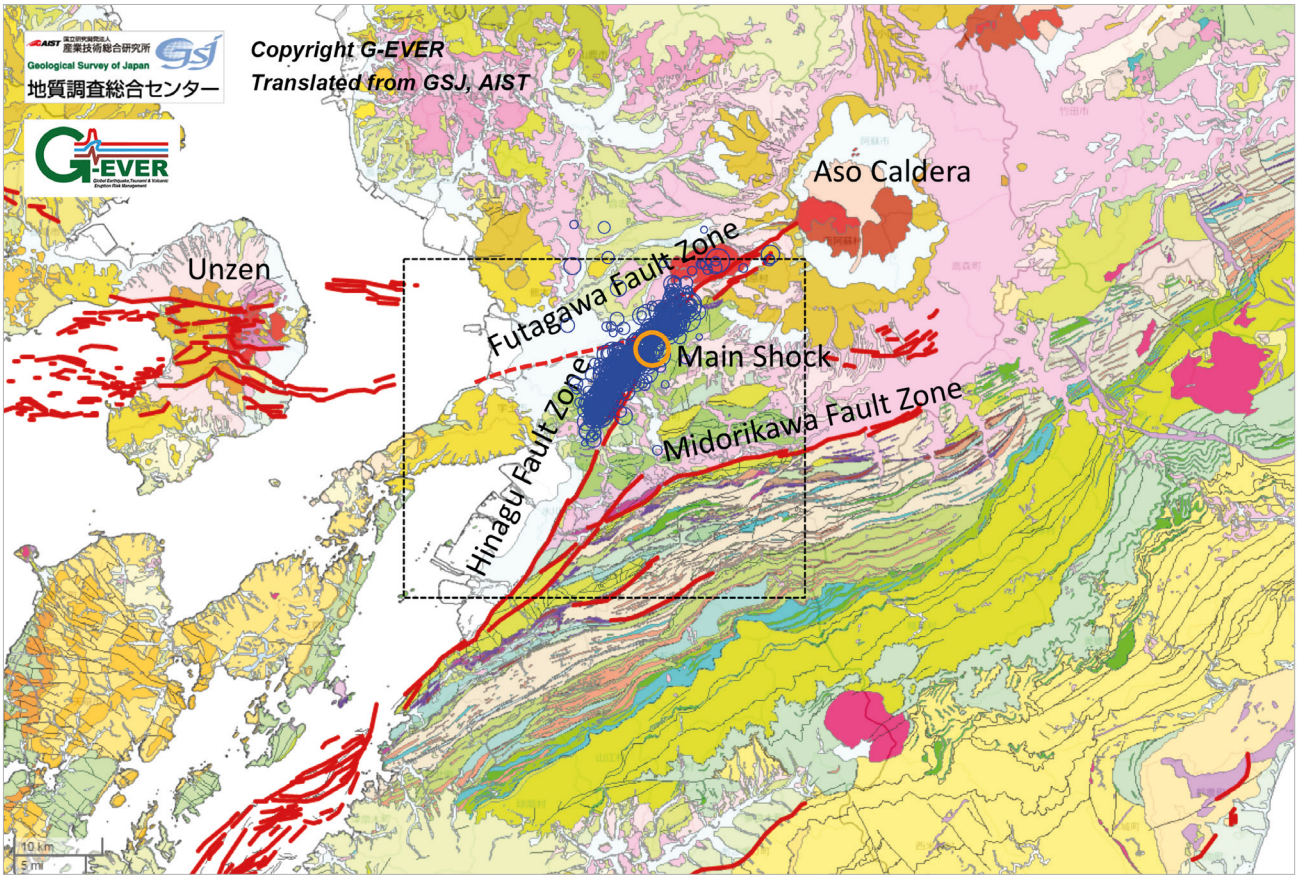

Fig. 2. Map of active faults in the area according to the Geological Survey of Japan [GSJ Volcanic Hazards..., 2021].

Рис. 2. Карта активных разломов района по данным геологической службы Японии [GSJ Volcanic Hazards..., 2021].

are confined. The Futagawa fault system becomes locked in the caldera of the active volcano Asosan in the north.

The study used the M>3 earthquake catalog obtained from the Internet archive of the National Earthquake Information Center of the US Geological Survey [Benz, 2017]. In view of the fact that the accuracy of determining the coordinates of the epicenters within the national seismic network of Japan is obviously higher than that obtained within the global seismic center, the coordinates of the epicenters of the main events were taken from [Kawamoto et al., 2016].

According to the Internet archive [Global Volcanism Program, 2021], during the GPS observations analyzed, the study area experienced the eruption of the Asosan volcano. The largest, VEI 2 eruption took place from August 30, 2014, to May 1, 2016, lasting somewhat less than 2 years.

4. CALCULATION OF ACCUMULATED DISPLACEMENT AND DEFORMATION OF THE EARTH'S SURFACE

The calculations of the horizontal displacements of GNSS points were based on time series obtained by the Nevada Geodetic Laboratory [Blewitt et al., 2018]. The horizontal displacements U_n and U_e were calculated for each day with respect to the initial epoch T_0, as the deviation between plane coordinates *n* and *e* in the UTM projection using the following formulas:

$$U_{n_i} = n_i - n_0,\ U_{e_i} = e_i - e_0$$

where index *i* denotes the current epoch of measurements.

Displacements of GNSS points in the global reference frame demonstrate primarily the trends in movement of the global tectonic plate on which the observation point is located. This effect makes it difficult to track smaller amplitude movements associated with local changes, such as slow accumulation of elastic deformations of the earth's crust near the epicenter of a future event. In this case, more indicative are the displacements of points presented in the local (inner) frame of reference, which reflect well the mutually divergent movements of the sides of local faults. Such a local (inner) reference frame of displacements can be easily obtained by subtracting the mean value $\bar{U}$, which characterizes the global tectonics trend typical of all network points, from each displacement U_j in the global reference frame for each measurement epoch. Thus, we get a frame of reference for displacements (or displacement rates) by "no net translation" conditions.

$$u_{n_i} = U_{n_i} - \bar{U}_n,\ u_{e_j} = U_{e_j} - \bar{U}_e$$

where index *j* is a sequentially numbered GNSS observation point.

Digital models of the distribution of the total horizontal shear deformation and dilatation were produced every day based on the displacement values. These characteristics are invariant with respect to the choice of the coordinate system.

The calculation of finite element deformations involved the horizontal strain tensor (with *n* and *e* axes directed to the north and east)

$$T_\varepsilon = \begin{pmatrix} \varepsilon_n & \varepsilon_{ne} \\ \varepsilon_{en} & \varepsilon_e \end{pmatrix},$$

whose elements were equal to $\varepsilon_n = \frac{\partial u_n}{\partial n}$, $\varepsilon_e = \frac{\partial u_e}{\partial e}$ and $\varepsilon_{en} = \varepsilon_{ne} = \frac{1}{2}\left(\frac{\partial u_n}{\partial e} + \frac{\partial u_e}{\partial n}\right)$, respectively,

where $\frac{\partial u_n}{\partial e} + \frac{\partial u_e}{\partial n} = \gamma_{ne} = \gamma_{en}$ is a relative shear.

The elements of the strain tensor are represented by partial derivatives of displacements u_n and u_e along the coordinate axes *n* and *e*.

To study spatiotemporal distribution of horizontal deformations, the following invariant characteristics were calculated:

1) Principal strains ε_1 and ε_2

$$\varepsilon_{1,2} = \frac{1}{2}\left[\varepsilon_n + \varepsilon_e \pm \sqrt{\left(\varepsilon_n - \varepsilon_e\right)^2 + \gamma_{ne}^2}\right];$$

2) Total shear $\gamma = \left(\left(\varepsilon_n - \varepsilon_e\right)^2 + \gamma_{ne}^2\right)^{1/2}$;

3) Dilatation $\Delta = \varepsilon_1 + \varepsilon_2$.

Strain components were calculated according to the method described in [Wu et al., 2006].

Due to strongly nonequidimensional finite elements (see Fig. 1), the deformation values were reduced to the average area of the network triangle [Kaftan, Melnikov, 2018].

In addition to the models of horizontal deformations, the unified analysis used the data on active faults in the study area [Kawamoto et al., 2016].

5. INTERPRETATION OF THE OBTAINED RESULTS

5.1. Analysis of movements and deformations in connection with generation of the strongest seismic events

Let us consider the pattern of the temporal change in the spatial distribution of horizontal and vertical displacements of the study area in connection with generation of the main seismic events. The corresponding visualizations are shown in Fig. 3.

Fig. 3, a, b, c, d show a slow accumulation of horizontal displacements, reaching nearly 10 cm a day before the first, M6.4 foreshock, and trending regularly northwest. At this time, the area undergoes negligible (up to –0.05 m) subsidence in its entirety and poorly defined uplifts in its southeastern part. These trends are consistent with the subduction mechanism of the Philippine Plate. Subsidence exceeded –0.05 m near the epicenters of strong foreshocks by the time

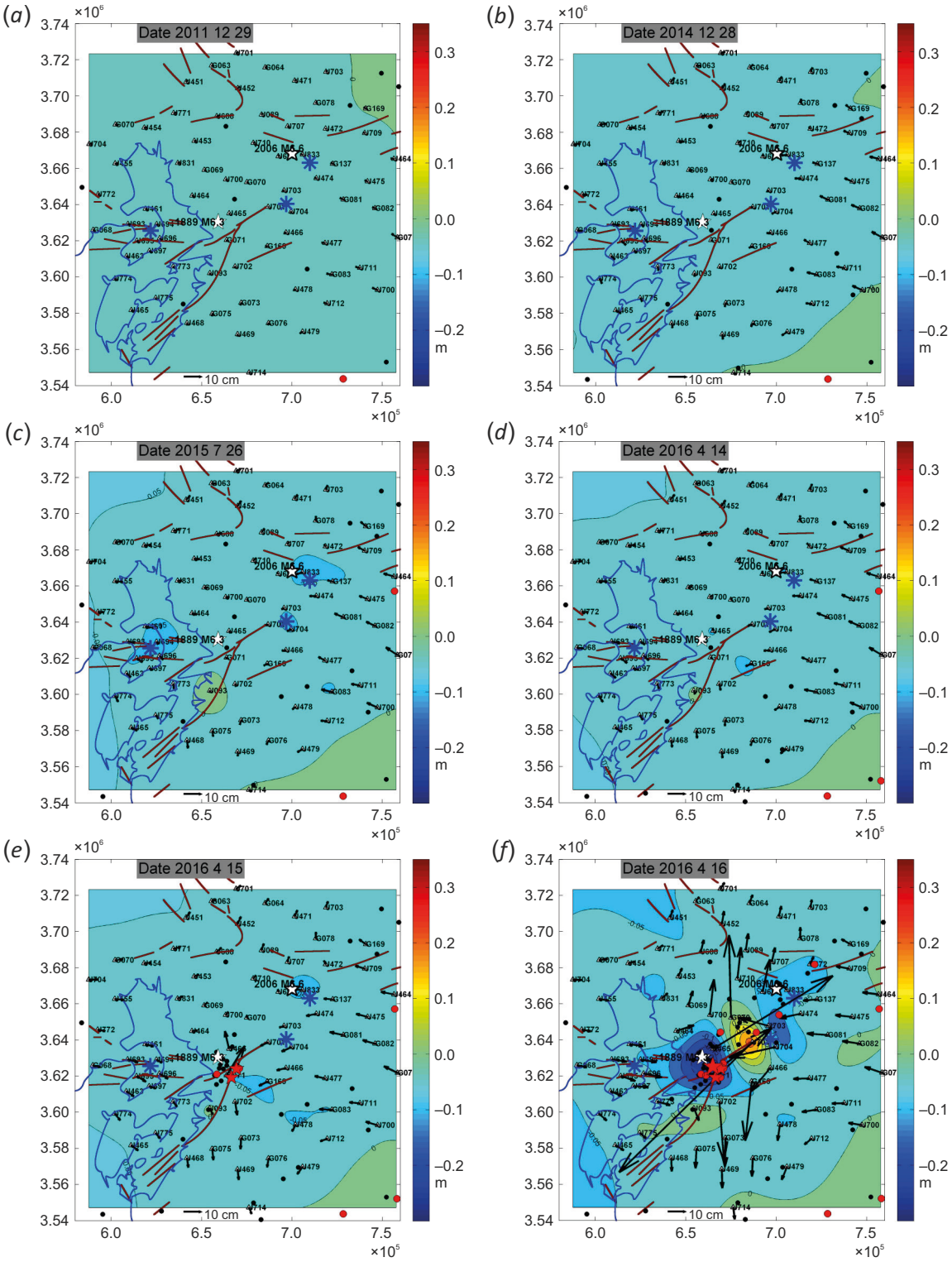

Fig. 3. Distribution of accumulated horizontal and vertical displacements before the 2016 Kumamoto earthquakes. The cross-section of isolines of vertical displacements is 5 cm. Color bars are presented on the right of the figures. Arrows stand for the vectors of horizontal displacements of the sites. See Fig. 1 for the legend of faults and seismic events. Black spots are small earthquakes. The rectangular coordinates on the frames of the figures are given in the UTM projection in meters.

Рис. 3. Распределение накопленных горизонтальных и вертикальных смещений перед землетрясениями Кумамото 2016 г.

Сечение изолиний вертикальных смещений – 5 см. Цветовые шкалы представлены справа от рисунков. Стрелки представляют собой векторы горизонтальных смещений пунктов. Легенду разрывных нарушений и сейсмических событий см. на рис. 1. Черные окружности – слабые землетрясения. Прямоугольные координаты на рамках рисунков даны в проекции UTM в метрах.

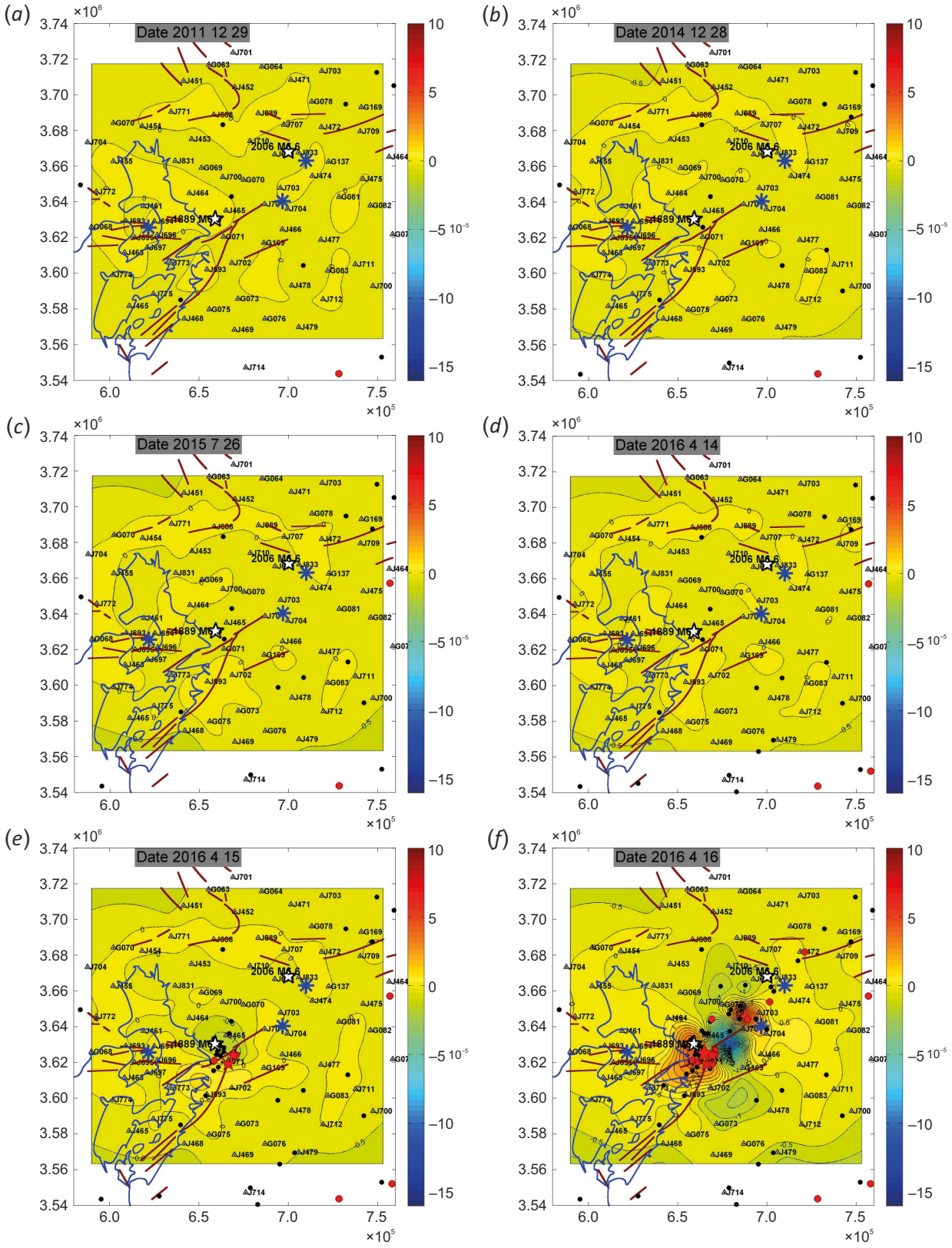

Fig. 4. Distribution of dilatation deformation before the 2016 Kumamoto earthquakes.
The cross-section of deformation isolines is $5 \cdot 10^{-6}$. See Fig. 1 for the legend of faults and seismic events. Black circles are small earthquakes. The rectangular coordinates on the frames of the figures are given in the UTM projection in meters.

Рис. 4. Распределение деформации дилатации перед землетрясениями Кумамото 2016 г.
Сечение изолиний деформации $5 \cdot 10^{-6}$. Легенду разрывных нарушений и сейсмических событий см. на рис. 1. Черные окружности – слабые землетрясения. Прямоугольные координаты на рамках рисунков даны в проекции UTM в метрах.

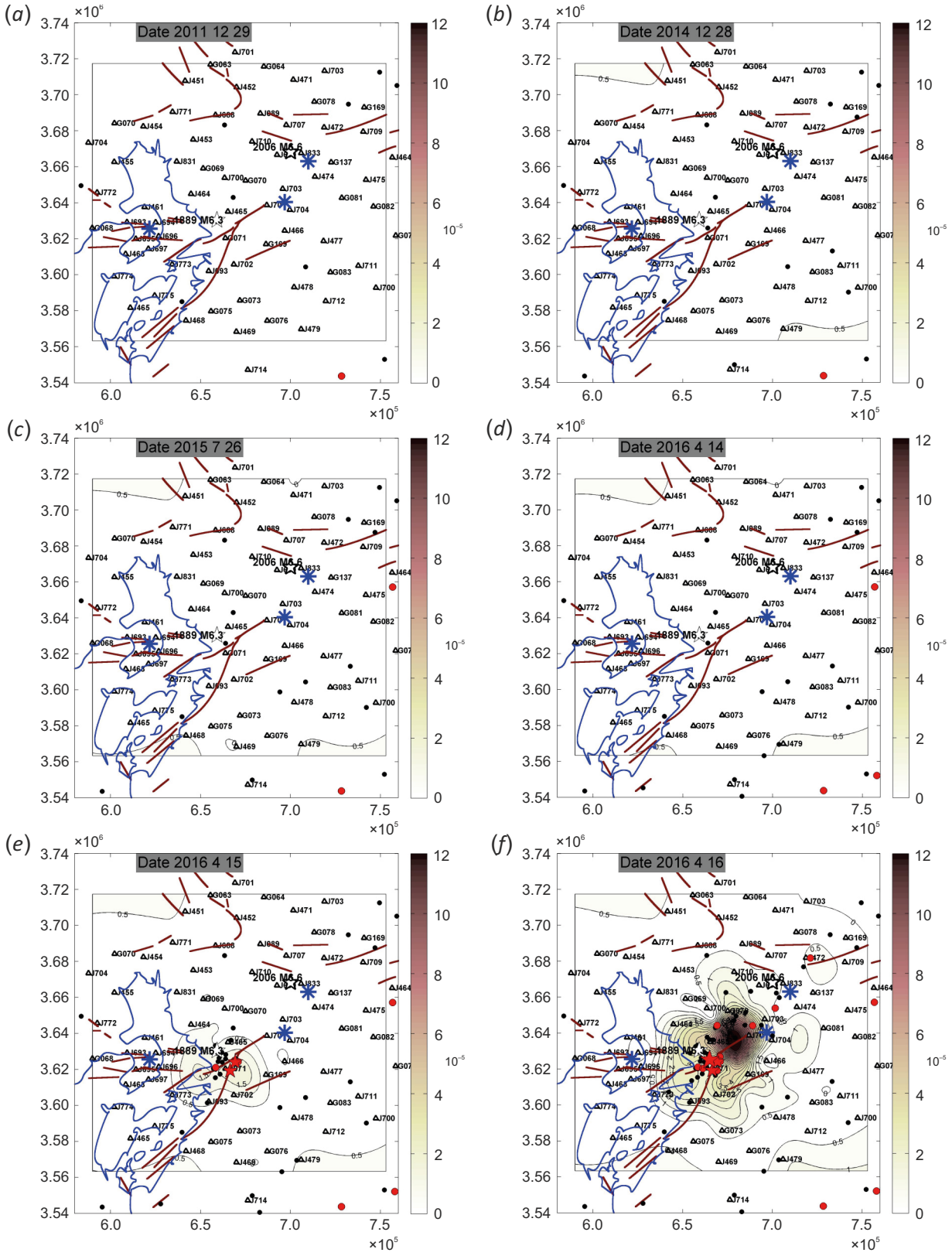

Fig. 5. Distribution of the total shear deformation accumulated before the Kumamoto earthquakes.
The cross-section of deformation isolines is $5 \cdot 10^{-6}$. See Fig. 1 for the legend of faults and seismic events. Black circles are small earthquakes. The rectangular coordinates on the frames of the figures are given in the UTM projection in meters.

Рис. 5. Распределение накопленной деформации полного сдвига перед землетрясениями Кумамото 2016 г. Сечение изолиний деформации $5 \cdot 10^{-6}$. Легенду разрывных нарушений и сейсмических событий см. на рис. 1. Черные окружности – слабые землетрясения. Прямоугольные координаты на рамках рисунков даны в проекции UTM в метрах.

of their occurrence. The vectors of horizontal displacements became somewhat longer. Coseismic horizontal and vertical displacements caused by the main (M7.3) shock are presented in Fig. 3, f. The most interesting facts therein were more than 1 m amplitude right-lateral strike-slip along the axial line of the Futagawa fault zone and the territories on both sides of seismic rupture moving simultaneously up to 1 m apart from each other. Surface uplift of more than 0.2 m occurred in the center of symmetry of the position emerged, just near to –0.2 m subsidence on both sides of the uplift. The extrema of vertical displacements are located on the axial line of the Futagawa fault zone.

Fig. 4 shows the evolution of dilatation based on some significant daily frames of the deformation process. As we can see from Figs. 4, a, b, c, d, there were no significant changes in dilatation in seven years prior to the main shocks. In the area of future epicenters, the day before the events, there occurred an insignificant extension of less than $5 \cdot 10^{-6}$. Against the background of nearby deformations, it is difficult to conclude about stress generation in the future earthquake source. Coseismic deformations are more pronounced. During strong foreshocks (Fig. 4, e), in the epicentral zone of the strongest foreshocks, there is evidence for the existence of compression anomaly of more than $1 \cdot 10^{-5}$ nearby the equal amount of extension southwest of the epicenters. During the main shock and foreshocks in this area, there occurred a significant extension of up to $1 \cdot 10^{-4}$ and a three-polar alternation with compression of up to $1.6 \cdot 10^{-4}$ and further extremum of extension along the strike of the Futagawa fault zone as a whole. It is worthy of note that this pattern is in good agreement with the pattern of vertical movements (see Fig. 3, f). It can be seen that uplifts are accompanied by compressions, and subsidence events are accompanied with extensions. These features demonstrate the mechanism of somewhat vertical hummocking of the upper layers of the earth's crust due to the stopping of fault-side ruptures after an intense right-lateral strike-slip and subsidence of adjacent territories under extension conditions.

The total shear deformation behavior is shown in Fig. 5. It is obvious that there were no significant shear deformations before strong foreshocks. They manifest themselves at $5 \cdot 10^{-6}$ level on the northwestern and southeastern margins of the study area (Fig. 5, d). There appears to be a regular trend accounting for general compression of this area owing to the mechanism of tectonic plate subduction. At the time of strong foreshocks, in their epicentral area there occurred the deformation (Fig. 5, e) at the level of $1.5 \cdot 10^{-5}$. The total shear deformation reached $1.2 \cdot 10^{-4}$ immediately after the main seismic event (Fig. 5, f). However, it was not in the zone of the epicenters of the Kumamoto series but moved to the northeastern part of the Futagawa fault zone, thereby demonstrating the direction of propagation of the seismic rupture.

5.2. Identification of a locked zone in the vicinity of the source of major earthquake

The use of a local (inner) reference system in relation to the accumulation of displacements of GNSS stations makes it possible to detect the zones of minimum mutual displacements. These zones mark the places of locally immobile areas of the earth's surface, typical for the locked zones of seismogenic faults [Kaftan, 2021; Kaftan et al., 2021]. The identification of slip deficit on seismogenic faults is done by different authors in order to determine the most seismically hazardous areas [Jiang et al., 2015; Wang et al., 2021]. Observations of the deformation process over the years and decades before strong seismic events show high stress regions –probable places expected strong crustal earthquakes whose come out to the daylight surface. According to Reid's elastic rebound hypothesis [Reid, 1911; Pevnev, 1988, 1989], the place of a future event is the "locked" zone of an active fault, in other words, the zone of minimal deformations in the area of earthquake generation. Such a zone in a seismically active area can be mapped based on the values of the total displacements of the GNSS points, which are the lengths of the vectors of horizontal displacements. The shorter the length of the displacement vector, the less mobile the earth's surface of the territory of its location. Based on the elastic rebound model, the place of the minimum movements in a seismically active area is the place of the maximum seismogenic stresses.

The evolution of the minimal displacements before the Kumamoto series is shown in Fig. 6, and also in the corresponding video [Kaftan, Shevchuk, 2021]. During a 7.3 year-long accumulation of deformation before the main seismic events, in the area of their future epicenters there occurred a zone of minimum (less than 0.02 m) displacements. These characteristics are the moduli of the vectors of accumulated displacements of GNSS points obtained by the formula:

$$u_i = \sqrt{u^2_{ni} + u^2_{ei}}.$$

After the occurrence of large events, the area of minimum displacements becomes destructed, forming white spaces on the images obtained (Fig. 6, e, f). These manifestations demonstrate the possibility of recording the area of expected strong seismic events, wherein intense coseismic shear deformations of the earth's surface occur as a result of an earthquake. We'll just have to understand more precisely the strain localization of strong future earthquakes in the areas extending for hundreds of kilometers. Note that the zone of minimal movements was not stable over time. It was localized gradually and disturbed by the earthquakes preceding more powerful events (Fig. 6, f).

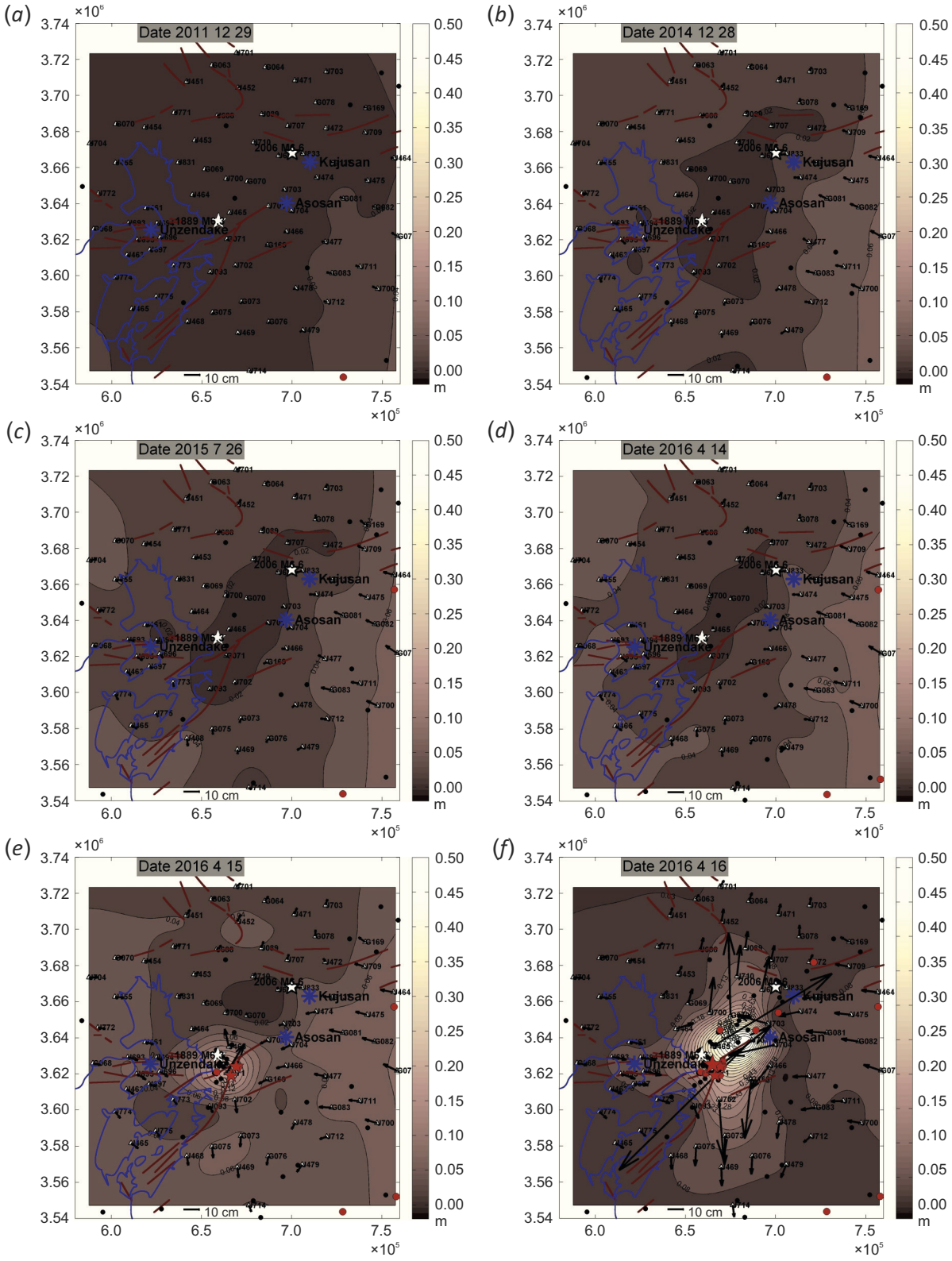

Fig. 6. Distribution of accumulated total displacements before the 2016 Kumamoto earthquakes.
The cross-sections of the total displacement isolines are 2 cm (*a, b,* c, *d, e*) and 5 cm (*f*). Arrows represent vectors of horizontal point displacements. See Fig. 1 for the legend of faults and seismic events. Black spots are small earthquakes. The rectangular coordinates on the frames of the figures are given in the UTM projection in meters.

Рис. 6. Распределение накопленных полных смещений перед землетрясениями Кумамото 2016 г.
Сечение изолиний полного смещения – 2 см (*a, b,* c, *d, e*) и 5 см (*f*). Стрелки представляют собой векторы горизонтальных смещений пунктов. Легенду разрывных нарушений и сейсмических событий см. на рис. 1. Черные окружности – слабые землетрясения. Прямоугольные координаты на рамках рисунков даны в проекции UTM в метрах.

This made it difficult to get a good estimate of the future strong earthquake location.

6. CONCLUSION

First of all, we would like to note that 127 years before the Kumamoto series of strong seismic events, a destructive M6.3 earthquake occurred in the vicinity of their epicentral zone. This circumstance gives an indication of the duration of elastic deformations accumulation before modern events, i.e., of the interseismic phase of the earthquake cycle. At the same time, the interval of GNSS observations of movements and deformations covers about 6 % of the entire duration of the seismic cycle, which in turn characterizes the degree of knowledge of the process of accumulation of deformations before strong events.

Consideration of the evolution of movements and deformations shows that there were no significant changes in their accumulation over the 7 years before the Kumamoto series. Prior to these seismic events, no evidence was found for deformation precursors or clearly pronounced trends in the deformation evolution characteristics. Of particular interest to this study is a comparison between the character of coseismic vertical movements and dilatation, especially pronounced in connection with the strongest seismic event (see Figs. 3, f; 4, f). In this situation, the maximum compression coincided with the low-rise transition zero isoline. The extremum of extension in the epicentral zone of the Kumamoto series coincided with the extremum of a well-pronounced subsidence. The uplift coincided with the compression-extension transition zero isoline approximately at the northeastern termination of the Futagawa fault zone – the place where the amount of material ejected by the Asosan volcano in 2014–2016 was fairly small. This was not accompanied by significant vertical or horizontal movements therein, prior to a series of strong events. The volcano's caldera was involved in a zone of intense deformations, after which the volcano stopped erupting during postseismic relaxation on May 1, 2016.

An area of considerable interest is almost entire absence of accumulation of significant deformations for seven years before the strong 2016 Kumamoto earthquakes. As noted above, clearly defined deformation inhomogeneties occurred for months and years before the earthquakes, in the strong motion generation areas in the contact zone of the North American and Pacific tectonic plates, [Kaftan, Melnikov 2017, 2018, 2019]. Such anomalies were not found for the Kumamoto series. At first glance, this inconsistency might be due to the fact that the Futagawa and Hinagu faults are far from the mobile contact zone of the Philippine and Eurasian tectonic plates, where the subduction rate reaches 6 cm per year [Zang et al., 2002]. They are located at a distance of about 300 km from this zone, while the strongest seismic events in Southern California occur directly in the contact zone of tectonic plates. This might explain the relatively low mobility of the studied zone.

The behavior of the minimum displacement moduli of the GNSS points is most interesting in relation to the development of movements and deformations during the stress accumulation before the Kumamoto series (Fig. 6). Analysis of the kinematics of this characteristic [Kaftan, Shevchuk, 2021] shows the formation of a localized area of minimum displacements (Fig. 6, d), within which the subsequent strongest seismic events fell. This fact demonstrates the possibility of identifying the location of future strong shocks based on the data from permanent GNSS network.

All identified features of movements and deformations characterize the kinematics of the median tectonic line of the axial zone of the southwestern part of the island arc of the Japanese archipelago. The combination of coseismic compression and uplift at the center of the formed triad of deformation extrema, as well as the consistency of subsidence with extensions at its edges, demonstrate the mechanism of growth of the central region of the island arc under compression and the role of volcanism in this process.

7. CONTRIBUTION OF THE AUTHORS

The authors contributed equally to this article.

Все авторы сделали эквивалентный вклад в подготовку публикации.

8. CONFLICT OF INTERESTS

The authors have no conflicts of interest to declare. All authors have read and agreed to the published version of the manuscript.

Авторы заявляют об отсутствии у них конфликта интересов. Все авторы прочитали рукопись и согласны с опубликованной версией.

9. REFERENCES

Active Fault Database of Japan, 2021. Available from: https://gbank.gsj.jp/activefault/index (Last Accessed September 14, 2021).

Benz H., 2017. Building a National Seismic Monitoring Center: NEIC from 2000 to the Present. Seismological Research Letters 88 (2B), 457–461. https://doi.org/10.1785/0220170034.

Blewitt G., Hammond W.C., Kreemer C., 2018. Harnessing the GPS Data Explosion for Inter-Disciplinary Science. Eos 99. https://doi.org/10.1029/2018EO104623.

Dahmen N., Hohensinn R., Clinton J., 2020. Comparison and Combination of GNSS and Strong-Motion Observations: A Case Study of the 2016 M_w 7.0 Kumamoto Earthquake. Bulletin of the Seismological Society of America 110 (6), 2647–2660. https://doi.org/10.1785/0120200135.

Global Volcanism Program, 2021. Available from: https://volcano.si.edu/ (Last Accessed September 1, 2021).

GSJ Volcanic Hazards Assessment Support System, 2021. http://g-ever1.org/quick/index_en.html (Last Accessed September 1, 2021).

He P., Wen Y., Xu C., Chen Y., 2019. Complete Three-Dimensional Near-Field Surface Displacements from Imaging Geodesy Techniques Applied to the 2016 Kumamoto Earthquake. Remote Sensing of Environment 232, 111321. https://doi.org/10.1016/j.rse.2019.111321.

Jiang G., Xu X., Chen G., Liu Y., Fukahata Y., Wang H., Yu G., Tan X., Xu C., 2015. Geodetic Imaging of Potential Seismogenic Asperities on the Xianshuihe-Anninghe-Zemuhe Fault System, Southwest China, with a New 3-D Viscoelastic Interseismic Coupling Model. Journal of Geophysical Research: Solid Earth 120 (3), 1855–1873. https://doi.org/10.1002/2014JB011492.

Johnston G., Riddell A., Hausler G., 2017. The International GNSS Service. In: P.J. Teunissen, O. Montenbruck (Eds), Springer Handbook of Global Navigation Satellite Systems. Springer-Verlag, Berlin, Heidelberg, p. 967–982. https://doi.org/10.1007/978-3-319-42928-1_33.

Kaftan V.I., 2021. An Analysis of Ground Movements and Deformations from 13-year GPS Observations before and during the July 2019 Ridgecrest, USA Earthquakes. Journal of Volcanology and Seismology 15 (2), 97–106. https://doi.org/10.1134/S0742046321010115.

Kaftan V.I., Kaftan I., Gök E., 2021. Crustal Movements and Deformations in Eastern Turkey in Connection with the Van Earthquake (October 23, 2011, M_w=7.2): Study from GPS Data. Izvestia, Physics of the Solid Earth 57 (3), 30–44. https://doi.org/10.1134/S1069351321030071.

Kaftan V., Melnikov A., 2017. Local Deformation Precursors of Large Earthquakes Derived from GNSS Observation Data. IOP Conference Series: Earth and Environmental Science 95 (3), 032030. https://doi.org/10.1088/1755-1315/95/3/032030.

Kaftan V.I., Melnikov A.Yu., 2018. Revealing the Deformational Anomalies Based on GNSS Data in Relation to the Preparation and Stress Release of Large Earthquakes. Izvestia, Physics of the Solid Earth 54, 22–32. https://doi.org/10.1134/S1069351318010093.

Kaftan V., Melnikov A., 2019. Migration of Earth Surface Deformation as a Large Earthquake Trigger. In: G. Kocharyan, A. Lyakhov (Eds), Trigger Effects in Geosystems. Springer Proceedings in Earth and Environmental Sciences. Springer, Cham, p. 71–78. https://doi.org/10.1007/978-3-030-31970-0_8.

Kaftan V., Rodkin M., 2019. Earth's Surface Deformation on Mount Etna: GPS Measurements, Interpretation, Relationship to the Mode of Volcanism. Journal of Volcanology and Seismology 13, 7–16. https://doi.org/10.1134/S0742046319010032.

Kaftan V., Shevchuk R., 2021. Massing of the Shear Deficit over the Seven Years before the 2016 Kumamoto Earthquake Series: Video. February 2021. http://doi.org/10.13140/RG.2.2.26662.65607.

Kato A., Nakamura K., Hiyama Y., 2016. The 2016 Kumamoto Earthquake Sequence. Proceedings of the Japan Academy 92 (8), 358–371. https://doi.org/10.2183/pjab.92.359.

Kawamoto S., Hiyama Y., Ohta Y., Nishimura T., 2016. First Result from the GEONET Real-Timeanalysis System (REGARD): The Case of the 2016 Kumamoto Earthquakes. Earth, Planets and Space 68, 190. https://doi.org/10.1186/s40623-016-0564-4.

Kubodera T., Suzuki T., Masaharu H., Matsuo E., 2017. Analysis on Surface Deformation and Cracks in Paddy Fields by 2016 Kumamoto Earthquake Using GNSS and Photogrammetry. International Journal of Environmental and Rural Development 8 (1), 85–92. https://doi.org/10.5194/nhess-17-143-2017.

Moore J., Yu H., Tang C., Wang T., Barbot S., Peng D., Masuti S., Dauwels J. et al., 2017. Imaging the Distribution of Transient Viscosity after the 2016 M_w 7.1 Kumamoto Earthquake. Science 356 (6334), 163–167. https://doi.org/10.1126/science.aal3422.

Nakajima J., Hasegawa A., 2007. Subduction of the Philippine Sea Plate beneath Southwestern Japan: Slab Geometry and Its Relationship to Arc Magmatism. Journal of Geophysical Research: Solid Earth 112 (B8). https://doi.org/10.1029/2006JB004770.

Pevnev A.K., 1988. Earthquake Prediction: Geodetic Aspects of the Problem. Izvestiya, Physics of the Solid Earth 12, 88–98.

Pevnev A.K., 1989. Deterministic Geodetic Prediction of Preparation Areas of Strong Crustal Earthquakes. Earthquake Prediction 11, 11–23.

Reid H.F., 1911. The Elastic-Rebound Theory of Earthquakes. Bulletin of the Department of Geology 6, 413–444.

Riznichenko Yu.V., 1992. Problems of Seismology: Selected Papers. Springer, Berlin, Heidelberg, p. 445.

Sagiya T., 2004. A Decade of GEONET: 1994–2003. The Continuous GPS Observation in Japan and Its Impact on Earthquake Studies. Earth Planets Space 56 (8), XXIX–XLI. https://doi.org/10.1186/BF03353077.

Tanaka Y., Ohta Y., Miyazaki S., 2019. Real-Time Coseismic Slip Estimation via the GNSS Carrier Phase to Fault Slip Approach: A Case Study of the 2016 Kumamoto Earthquake. Geophysical Research Letters 46 (3), 1367–1374. https://doi.org/10.1029/2018GL080741.

Wang K., Zhu Y., Nissen E., Shen Z.-K., 2021. On the Relevance of Geodetic Deformation Rates to Earthquake Potential. Geophysical Research Letters 48 (11), e2021GL093231. https://doi.org/10.1029/2021GL093231.

Wu J.C., Tang H.W., Chen Y.Q., Li Y.X., 2006. The Current Strain Distribution in the North China Basin of Eastern China by Least-Squares Collocation. Journal

of Geodynamics 41 (5), 462–470. https://doi.org/10.1016/j.jog.2006.01.003.

Yamagiwa S., Miyazaki S., Hirahara K., Fukahata Y., 2015. Afterslip and Viscoelastic Relaxation Following the 2011 Tohoku-Oki Earthquake (M_w9.0) Inferred from Inland GPS and Seafloor GPS/Acoustic Data. Geophysical Research Letters 42 (1), 66–73. https://doi.org/10.1002/2014GL061735.

Yang Y., Qin X., 2021. Resilient Observation Models for Seafloor Geodetic Positioning. Journal of Geodesy 95, 79. https://doi.org/10.1007/s00190-021-01531-7.

Zang S.X., Chen Q.Y., Ning J.Y., Shen Z.K., Liu Y.G., 2002. Motion of the Philippine Sea Plate Consistent with the NUVEL-1A Model. Geophysical Journal International 150 (3), 809–819. https://doi.org/10.1046/j.1365-246X.2002.01744.x.